Modeling the Bending of Probes Used in Semiconductor Industry

Alain R. Comeau, *Member, IEEE,* and Normand Nadeau, *Member, IEEE*

***Abstract*—An analytical model for the bending of probes used in the semiconductor industry is presented. It is shown that tip sliding distance is twice as large as it was previously believed. This difference is shown to be caused by the beam curvature which increases the angle between the tip and the vertical, and pushes the tip forward. Our model uses the probe shape and the material elastic properties to estimate the beam curvature. Tip sliding distance, force and tip angle variance are calculated as a function of beam dimensions and overdrive. The model is in agreement with sliding distance measured by scanning electron microscopy (SEM).**

Introduction

FOR most probe users, one basic parameter is of interest: contact resistance. Those having to probe devices with more than 20 pads are concerned with the force applied on the probes, because the force can bend the probe card. Probe planarization is very important in this case, and will not be discussed in this paper.

The tip forward displacement is an important parameter; for long, it has been considered to be 0.1 μm/μm of overdrive [1]. This value was obtained by considering the beam length (L_B), about 5080 μm, and the beam angle with the horizontal axis (θ_B), about 7°. Upon overdrive, the beam was considered to behave like a rigid bar with a pivot at its attach point.

Questions were raised when it was found that the actual forward tip displacement lies between 0.2 and 0.3 μm/μm of overdrive [2]. The model presented here shows that bending the beam induces a forward displacement of 0.1 μm/μm of overdrive in agreement with Lee's results [1]. However, we show that the tip angle is increased by the beam bending. The tip angle increase pushes the tip further ahead and increases the sliding distance, confirming the results of Nadeau *et al.* [2]. This paper shows how we arrive at such conclusion using conventional solid mechanics.

Theory

The probe dimensions are defined in Fig. 1. We assumed that the probe is cylindrical in shape and has a cone beginning at a distance L_C from the attach point (taper length = $L_B - L_C$). The cone is considered to be regular up to the tip. The probe material modulus of elasticity (E) is believed to be constant over the beam length.

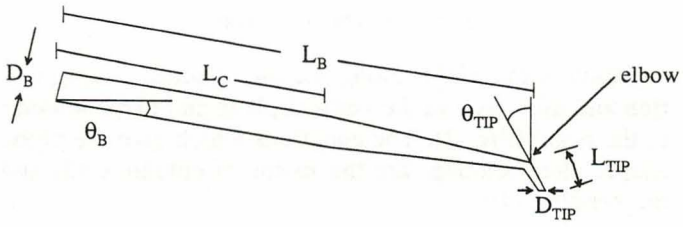

D_B	**Beam diameter**
L_B	**Beam length**
θ_B	**Beam angle**
L_B-L_C	**Taper length**
D_{TIP}	**Tip diameter**
L_{TIP}	**Tip length**
θ_{TIP}	**Tip angle**

Fig. 1. Probe shape parameters definition. It is assumed that cone is regular up to tip.

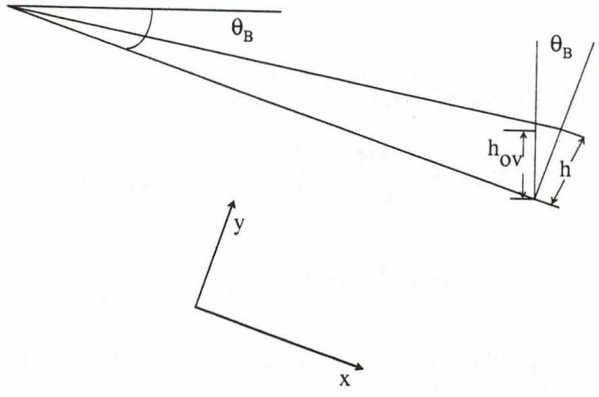

Fig. 2. Perpendicular displacement (h) as result of vertical overdrive (h_{ov}); x-axis is rotated θ_B from horizontal plane.

To insure contact during probing, an overdrive ($h_{ov} \cong 100$ μm) is applied after wafer surface detection by a sensing device. This is small compared to the beam length ($L_B \cong 5000$ μm). For such small overdrive distance, the probe displacement along the y axis (h) is approximately given by (1):

$$h \cong \frac{h_{ov}}{\cos(\theta_B)}. \tag{1}$$

Manuscript received June 4, 1990; revised November 30, 1990.

The authors are with Mitel Semiconductor, 18 Blvd. de l'Aeroport, Bromont, PQ, Canada J0E 1L0.

IEEE Log Number 9042449.

For an elastic material we have:

$$M = \frac{EI}{\rho} \tag{2}$$

M = bending moment

E = modulus of elasticity

ρ = radius of curvature

I = moment of inertia.

Defining the x axis along the initial probe beam position and the y axis in the vertical plane and perpendicular to the beam (Fig. 2). The equations which give the probe shape, after bending, are the radius of curvature (3) and the bending (4):

$$\frac{1}{\rho} = \frac{\dfrac{\partial^2 y}{\partial x^2}}{\left[1 + \left(\dfrac{\delta y}{\delta x}\right)^2\right]^{3/2}} \tag{3}$$

$$\frac{\partial^2 M}{\partial x^2} = P(x). \qquad P(x) = \text{force per unit length} \tag{4}$$

In our case, the force is concentrated at the tip, through the external force $(-F)$; we can approximate $P(x)$ by

$$P(x) = -F \cdot \delta(x - L_B) \tag{5}$$

where $\delta(x)$ is the Dirac function. Using (4) and (5), the shearing force $V(x)$ on the beam is

$$V(x) = \frac{-\partial M}{\partial x} = \int_0^x F \cdot \delta(x - L_B)\, dx$$

$$= F \int_0^x \delta(x - L_B)\, dx + C_1. \tag{6}$$

Knowing that $V(L_B) = 0$, we have $C_1 = -F$. Integrating again, we find M:

$$M = \int_0^x F\, dx = -Fx + C_2 \tag{7}$$

using (2):

$$M = EI(x) \cdot \left[\frac{\dfrac{\partial^2 y}{\partial x^2}}{\left[1 + \left(\dfrac{\partial y}{\partial x}\right)^2\right]^{3/2}}\right] = -Fx + C_2. \tag{8}$$

The beam curvature must vanish at L_B. Therefore, we have for C_2 and M:

$$C_2 = FL_B \tag{9}$$

$$M = F(L_B - x) \tag{10}$$

substituting (10) in (8), we find

$$I(x)\left[\frac{\dfrac{\partial^2 y}{\partial x^2}}{\left[1 + \left(\dfrac{\partial y}{\partial x}\right)^2\right]^{3/2}}\right] = \frac{F}{E}(L_B - x). \tag{11}$$

$I(x)$ is the beam cross-section inertia along the y-axis, taken at point x. $I(x)$ can be simply expressed on the basis that the beam is cylindrical at all points along the x axis and by approximating the force direction as being parallel to the y axis. Under these conditions, $I(x)$ is given by (12):

$$I(x) = \frac{\pi}{64} d(x)^4 \qquad d(x) = \text{beam diameter at point } x \tag{12}$$

Using (11), we find

$$\frac{\partial^2 y}{\partial x^2} = 64 \frac{F}{E} \frac{(L_B - x)}{\pi d(x)^4} \cdot \left[1 + \left(\frac{\partial y}{\partial x}\right)^2\right]^{3/2}. \tag{13}$$

Equation (13) is the probe bending solution. It can be simplified for small deviations from the horizontal plane. In this case, the last term can be dropped as the first derivative is small, and (13) becomes

$$\frac{\partial^2 y}{\partial x^2} = \frac{64}{\pi} \frac{F}{E} \frac{(L_B - x)}{d(x)^4}. \tag{14}$$

This equation gives the probe shape as it is bent under force F. If one were to keep the quadratic first derivative term in (13), the correction to the second derivative would be about 1%. Under the current approximations, the curvature $(1/\rho)$ is given by (14).

Our model does not impose a constant beam length; therefore, we incorrectly elongate the beam (Fig. 3). To correct this elongation, we calculate the resulting elongated beam length (L_B'), given by (15), and make the following calculation using this length instead of original beam length:

$$L_B' = \int_0^{L_B} \left(1 + \left(\frac{\partial y}{\partial x}\right)^2\right)^{1/2} dx. \tag{15}$$

To find the elbow displacement induced by the bending, we have to take into account the angle between the beam and the horizontal plane (θ_B). The projected beam length (Λ_B) at this angle is

$$\Lambda_B = \int_0^{L_B} \cos\left(\theta_B - atn\left(\frac{\partial y}{\partial x}\right)^2\right) dx. \tag{16}$$

The elbow displacement (17) is the difference between the bent beam length (Λ_B) and the beam length at rest (L_B'), projected on the horizontal plane (Fig. 4). This difference could be corrected for beam elongation, but the correction would be proportional to the theoretical elongation itself (less than 1%), and is neglected for relatively small bending angles.

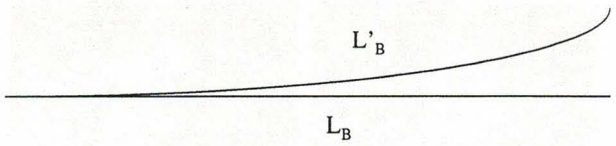

Fig. 3. Comparison between beam length used (L_B) and resulting beam length after bending (L'_B) calculating using model. Model incorrectly elongates beam; Correction to beam length is made by calculating beam elongation.

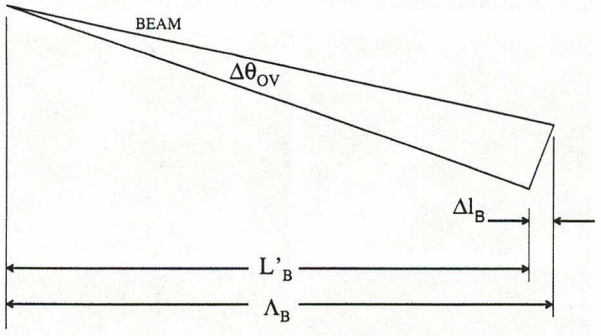

Fig. 4. Elbow displacement (Δl_B) under change in beam angle ($\Delta\theta_{ov}$) relative to horizontal plane. Λ_B is bent beam projected length on horizontal plane. L'_B is beam length at rest, projected on horizontal plane.

Therefore, the total displacement is separated in two components:

a) The elbow displacement induced directly by the overdrive (Δl_B), and given by (17):

$$\Delta l_B \cong \Lambda_B - L'_B \cdot \cos(\theta_B). \tag{17}$$

This result agrees well with Lee [1].

b) The displacement, induced by the tip angle change ($\Delta\theta_{TIP}$) and caused by beam bending near the elbow, is given by (19) for small angles (see Fig. 5):

$$\Delta l_{TIP} = L_{TIP} \cdot \sin\left(\theta_{TIP} + atn\left(\frac{\partial y}{\partial x}\right)_{L_B}\right) - \sin(\theta_{TIP}) \tag{18}$$

$$\Delta l_{TIP} \cong L_{TIP} \cdot \left(\frac{\partial y}{\partial x}\right)_{L_B}. \tag{19}$$

The model asumes that the tip does not deform under force and that the angle between the beam and the tip remains constant under bending. The former is easily accepted, because of the large ratio D_{TIP}/L_{TIP} and because the perpendicular force on the tip is small. The elbow angle stability is less obvious and depends on manufacturing quality; soft tips are known to have detrimental characteristics because they suffer from cracks in the elbow.

Variation in beam slope at the elbow causes the tip angle to change. This change may be such that the tip will rest on its heel at the end of overdrive. The reduced contact area, in this case, is detrimental to contact resistance

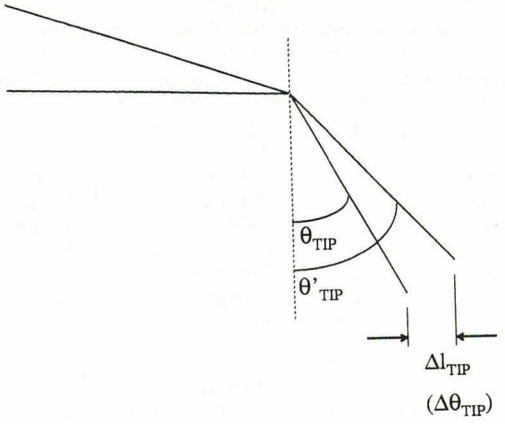

Fig. 5. Tip-elbow displacement (Δl_{TIP}) induced by tip angle change ($\Delta\theta_{TIP}$).

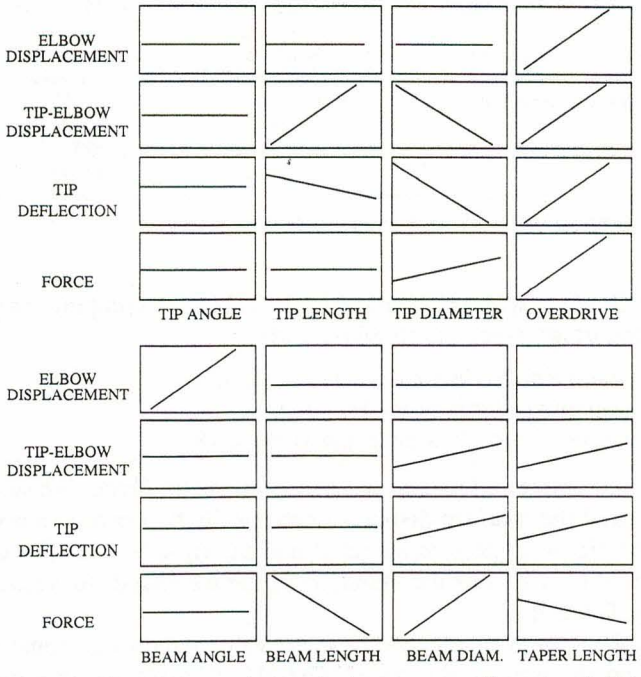

Fig. 6. Condensed picture showing basic parameters (dimensions in Table I) as function of seven basic geometric characteristics and overdrive. Effect of each geometric characteristic is shown as simplified graph. Steeper slope, more important effect is.

and may damage the pad. The final angle by which the tip is raised is

$$\Delta\theta_{TIP} = ATN\left(\frac{\partial y}{\partial x}\right)_{L_B} \sim \left.\frac{\partial y}{\partial x}\right|_{L_B} \tag{20}$$

This angle lifts the probe tip nose by a distance of

$$D_{TIP} \cdot \left.\frac{\partial y}{\partial x}\right|_{L_B}. \tag{21}$$

Case Analysis

The probe described in Table I is commonly used in the semiconductor industry. We used (1), (14)–(17), (19), and

TABLE I
STANDARD AND IMPROVED PROBED DIMENSIONS

Characteristics		Standard	Improved
Material = tungsten	E	3.5×10^{11} N/m^2	3.5×10^{11} N/m^2
Beam angle	θ_B	7°	4°
Beam length	L_B	5080 μm	5080 μm
Beam diameter	D_B	254 μm	152 μm
Taper length	L_B-L_C	2540 μm	635 μm
Tip angle	θ_{TIP}	7°	7°
Tip length	L_{TIP}	254 μm	127 μm
Tip diameter	D_{TIP}	50.8 μm	50.8 μm

TABLE II
PROBE MOVEMENT SENSITIVITIES FOR PROBES DEFINED IN TABLE I

Parameters	Standard	Improved
Total sliding distance	0.24 μm/μm overdrive	0.09 μm/μm overdrive
Elbow displacement	0.10 μm/μm overdrive	0.05 μm/μm overdrive
Tip-elbow displacement	0.14 μm/μm overdrive	0.04 μm/μm overdrive
Tip angle deflection	0.031°/μm overdrive	0.0173°/μm overdrive
Force	0.0012 N/μm overdrive	0.00020 N/μm overdrive

Improved probe shows reduced sliding distance and reduced force.

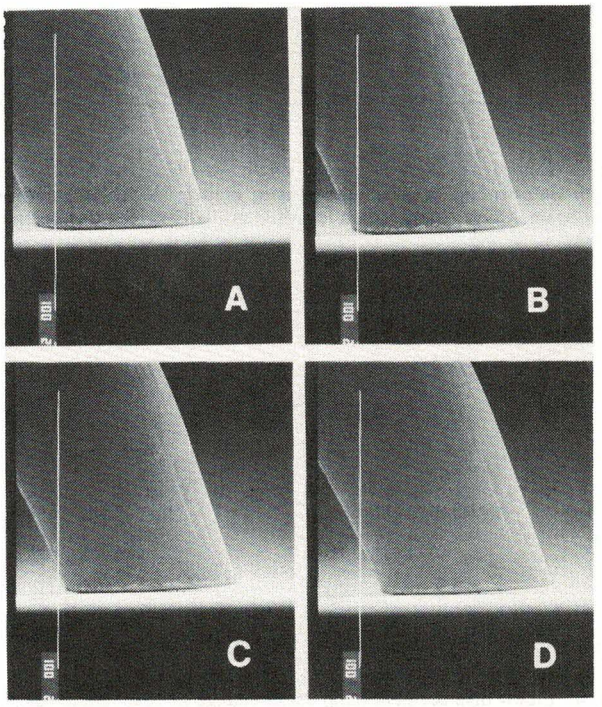

Fig. 7. Gradual decrease in tip contrast surface and tip sliding. Substrate was oxidized silicon wafer. A is at contact, B for 25-μm overdrive, C for 50-μm overdrive and D for 75-μm overdrive. Vertical bar is 100-μm long. Sliding distance for 75-μm overdrive is 14.2 $\pm$ 0.5 μm.

(20) along with the dimensions in Table I to compute three important probe parameters, namely:

total tip displacement ($\Delta l_B + \Delta l_{TIP}$)
tip angle deflection ($\Delta\theta_{TIP}$)
force perpendicular to the surface (F).

To better understand the mechanisms involved, we separated the total tip displacement into its two components: the elbow displacement (Δl_B) and the tip-elbow displacement (Δl_{TIP}). For the standard probe we found the values in Table II.

The elbow displacement is the value which was considered to apply to the tip by Lee [1]. We can see that our results agree perfectly with the accepted value (.1 μm/μm). We also see the tip-elbow displacement is as large as elbow displacement; this explains the results obtained by Nadeau *et al.* [2].

Standard probe characteristics were varied 10 to 50% about their targeted value and the four probe tip parameters were studied to determine their relative sensitivity. The results are summarized in Fig. 6.

Interesting features can be highlighted from Fig. 6:

1) Except for one case, the tip-elbow displacement and the probe tip deflection vary in the same manner, as expected from (19).
2) Because the tip is almost vertical, varying the tip angle has little effect on probe characteristics.
3) Probe tip parameters are proportional to overdrive.
4) The tip diameter has a very strong influence on the probe tip deflection. The tip diameter controls the elbow diameter. Since bending depends on $d(x)^{-4}$, beam bending (near the elbow) is reduced when tip diameter is increased.
5) The beam angle (θ_B) has a strong effect only on elbow displacement, as shown by (22):

$$\Delta L_a \sim h_{ov} \cdot \sin(\theta_B). \tag{22}$$

6) Beam length and diameter mainly affect the force on probe tip. These effects are explained by the cylindrical beam equation [3]. The force is proportional to D_B^4 and inversely proportional to L_B^3. These are very sensitive variables:

$$\frac{F}{E} = \frac{3\pi}{64}\frac{hD_B^4}{L_B^3}. \tag{23}$$

7) The taper length ($L_B - L_C$) has intermediate effect on most parameters.

Probe material change would only modify the force applied. All other parameters are of geometric nature and do not change. The force will vary linearly with the modulus of elasticity.

Fig. 7 presents SEM pictures of a typical probe taken at different stages of overdrive. This probe had standard dimensions except for tip length (140 μm instead of 254 μm) and tip diameter (62 μm instead of 50.8 μm). The surface was an oxidized silicon wafer. The vertical white bar is 100-μ long. Using this bar as a reference, the tip sliding is easily measured. From such SEM pictures taken at overdrive increments of 10 μm, we measured sliding distance versus overdrive.

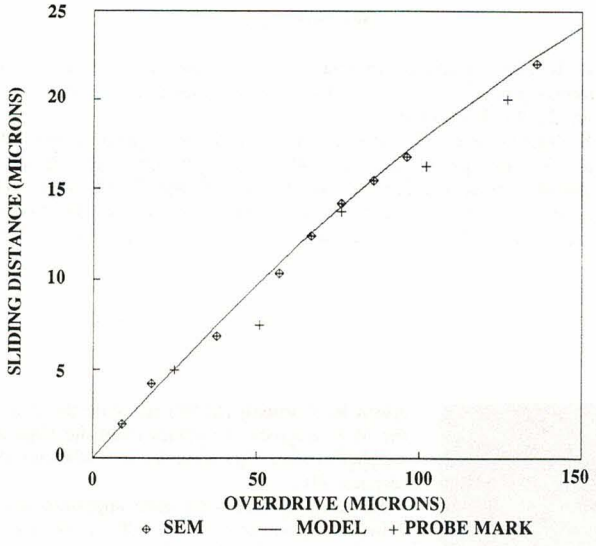

Fig. 8. Tip sliding distance given by model (solid line), scanning electron microscopy measurement (lozenges), and probe mark measurements. Probe was standard (Table I), except for a shorter tip length (140 μm). Agreement between model and SEM measurements is excellent.

Fig. 8 shows sliding distance measured from SEM picture, versus the model calculation. Sliding distance measurements from probe mark optical photographs are also presented in Fig. 8. The agreement with the SEM picture measurements is well within 1.5 μm. The probe mark data are more scattered because of measurement difficulty.

With this model, the geometrical parameters can be varied to fit any requirements for sliding distance, force or tip angle. For example, if one would like to decrease the total sliding distance and apply less force, an improved probe design could be used (Table I).

The improved probe response is shown in Table II. The material used was tungsten. The force applied by the probe was lowered by decreasing the beam diameter. The tip-elbow displacement was decreased by using the a shorter tip and a shorter taper. The elbow displacement was lowered by making the beam angle more shallow. Less damage is expected from the improved probe because the mechanical work done on the pad is reduce (force X sliding distance X friction coefficient).

Discussion on Contact Resistance and Pad Damage

For probe users, the following criteria are most important:

contact resistance
probe mark length
probe mark depth
pressure on the bonding pad.

Contact resistance is important for trivial reasons. A low resistance must be achieved by the contact area at the end of probe sliding, as postulated in Fig. 9. The slide length should not extend outside the pad and should be as small as possible to reduce the abrasion. The probe mark

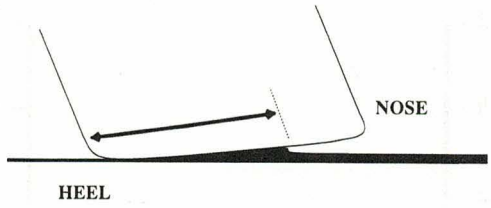

Fig. 9. Scraping of soft pad material like aluminum. Contact area is expected to remain nearly constant, as pile up of pad material at heel compensates for increase in tip angle which lifts nose.

depth is important because the probing action pushes the material off the pad. In such case, it is preferable to have a very uniform and nearly flattened tip to spread the force over the largest area [2]. A minimal sliding distance is desirable in all cases. Too much overdrive will push more metal off the pad. Decreasing the force applied by the probe obviously helps.

Pressure, probe tip deflection and sliding distance are determinant to contact resistance and to pad damage. The distributed pressure on the pad is determined by local resulting force and by the contact area. The contact area is determined by pad material plastic deformation and contact surface shape.

Slight tip rounding is desirable to avoid pad damage caused by sharp edges on the tip. If the tip is too flat, the force applied, at the end of overdrive, will be on a very small contact area (tip heel in Fig. 9), and the pressure on the pad will become very large (about 10^8 N/m^2). In these circumstances, damage to the aluminum, to the material underneath or to the tip may occur (cracks, material removal). Good tip rounding is obtained with proper sanding technique and adequate choice of sanding paper grain size [2].

Hard surfaces are usually not probed on device, however such surfaces are often used to verify contact resistance on planarization and probe mounting equipment. We found that this hard material is not sufficiently polished to offer reliable resistance measurement. In Fig. 10, a typical hard surface is compared to aluminum, approximately 1-μm thick on silicon.

The typical surfaces found on these equipment is very rough compared to the well polished tip contact area. In this case, the probe tip makes contact only with bumps; giving an erratic resistance, and damaging the tip. The erratic contact resistance on hard surfaces is unacceptable. Probing on a silicon wafer coated with 1-μm aluminum layer resolves this problem and is representative of real pad material surface. The contact resistance on aluminum decreases with increasing overdrive as the aluminum is pushed underneath the probe tip during the forward displacement. This causes the contact area to grow, as in Fig. 9.

Conclusion

It was shown that probes used today behaves like an elastic beam. Our model showed that the tip displacement and the tip deflection angle solely depend on probe shape

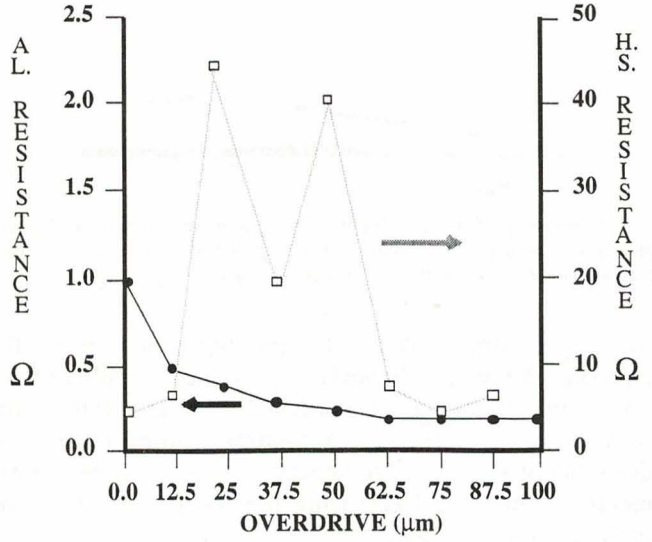

Fig. 10. Contact resistance versus overdrive on hard surface (H.S.) and on 1-μm thick aluminum layer on silicon (AL.). Left scale is for aluminum, right scale is for hard surface.

and overdrive. We calculated the tip displacement for a standard probe to be 0.24 μm/μm of overdrive, in accordance with measured values. From probe sliding distance and force requirements, the model can be successfully used to design probes. We noted the importance of tip angle deflection for contact resistance and pad damage. We also showed that the use of poorly polished hard surfaces to verify contact resistance should be banned, as it does not represent the reality of pad material being pushed off underneath the tip and yield erratic contact measurement.

Acknowledgement

The authors would like to thank Mitel S.C.C. to allow publication of this work, Yves Tremblay for the SEM pictures, and the reviewers for their constructive comments.

References

[1] D. B. Lee, "Linking semiconductor fabrication and assembly via automation," *Microelectronic Manfacturing and Testing*, vol. 9, no. 2, pp. 20–23. Feb. 1986.

[2] N. Nadeau and S. Perreault, "An analysis of tungsten probes effects on yield in a production wafer probe environment," *Microelectronic Manufacturing and Testing*, vol. 12, no. 10, pp. 35–37. Sept. 1989.

[3] E. Popov, *Introduction to the Mechanics of Solids*, N. M. Newmark and W. J. Hall, Eds. Englewood Cliffs, NJ: Prentice-Hall, 1968.

*

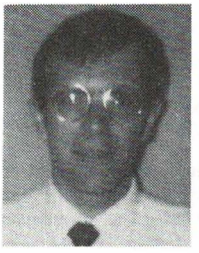

Alain R. Comeau (M'90) received the B.S. and the M.S. degrees in physics from the University of Sherbrooke, PQ, Canada, in 1984 and 1989, respectively.

He has held three work terms appointments with Mitel Semiconductor from 1983–1984, and was awarded an NSERC scholarship for one of his work terms (1983), and an FCAR scholarship for his M.S. degree (1985–1987). In 1988 he joined Mitel as a member of the Process Yield Improvement Group. His research interests include yield modeling, gettering in epitaxial silicon wafers, defect monitoring tests chips, 1/f noise and integrated circuit probing.

Mr. Comeau has a patent pending in Canada and in the United States for a test chip which can electrically locate and identify defects on itself.

*

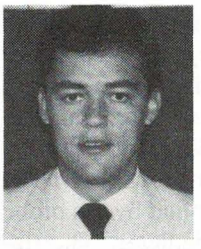

Normand Nadeau (M'89) received the D.E.C. degree in electronics from CEGEP de Sherbrooke, PQ, Canada, in 1980.

He has more than ten years of experience in the wafer test department at Mitel Semiconductor, where he was responsible for the repair of equipment to increase productivity. He has also had some experience in training technical personnel at MEDL (Marconi Electronic Device Limited) in England.

Mr. Nadeau currently has a patent application pending in Canada and in the United States for a low profile inker for high frequency test heads.